AD-A135 563 COMPUTER CALCULATIONS OF PIN DIODE LIMITER CHARACTERISTICS(U) HARRY DIAMOND LABS ADELPHI MD A L WARD SEP 83 HDL-TR-2124 1/1

UNCLASSIFIED F G 9/1 NL

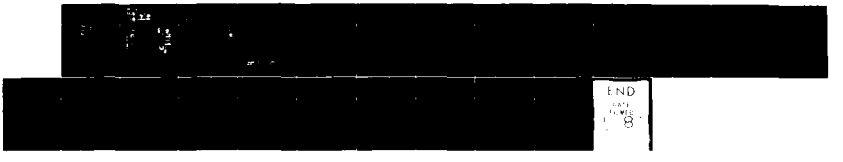

END
DATE FILMED
1-84
DTIC

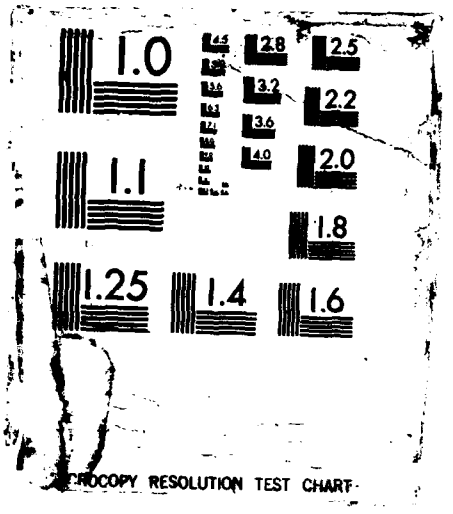
1.0
1.1
1.25
1.4
1.6
2.8
3.2
3.6
4.0
2.5
2.2
2.0
1.8
ROCOPY RESOLUTION TEST CHART

HDL-TR-2124
September 1987

Computer Calculations of PIN Diode Limiter Characteristics

by Alford L. Ward

U.S. Army Laboratory Command
Harry Diamond Laboratories
Adelphi, MD 20783-1197

The findings in this report are not to be construed as an official Department of the Army position unless so designated by other authorized documents.

Citation of manufacturers' or trade names does not constitute an official indorsement or approval of the use thereof.

Destroy this report when it is no longer needed. Do not return it to the originator.

UNCLASSIFIED
SECURITY CLASSIFICATION OF THIS PAGE

REPORT DOCUMENTATION PAGE

1a. REPORT SECURITY CLASSIFICATION UNCLASSIFIED	1b. RESTRICTIVE MARKINGS
2a. SECURITY CLASSIFICATION AUTHORITY	3. DISTRIBUTION / AVAILABILITY OF REPORT Approved for public release; distribution unlimited.
2b. DECLASSIFICATION / DOWNGRADING SCHEDULE	
4. PERFORMING ORGANIZATION REPORT NUMBER(S) HDL-TR-2124	5. MONITORING ORGANIZATION REPORT NUMBER(S)
6a. NAME OF PERFORMING ORGANIZATION Harry Diamond Laboratories 6b. OFFICE SYMBOL (If applicable) SLCHD-NW-RE	7a. NAME OF MONITORING ORGANIZATION
6c. ADDRESS (City, State, and ZIP Code) 2800 Powder Mill Road Adelphi, MD 20783-1197	7b. ADDRESS (City, State, and ZIP Code)
8a. NAME OF FUNDING / SPONSORING ORGANIZATION U.S. Army Laboratory Command 8b. OFFICE SYMBOL (If applicable) AMSLC	9. PROCUREMENT INSTRUMENT IDENTIFICATION NUMBER
8c. ADDRESS (City, State, and ZIP Code) 2800 Powder Mill Road Adelphi, MD 20783-1145	10. SOURCE OF FUNDING NUMBERS PROGRAM ELEMENT NO. 62120A PROJECT NO 1L162120 A140 TASK NO. WORK UNIT ACCESSION NO.
11. TITLE (Include Security Classification) Computer Calculations of PIN Diode Limiter Characteristics	
12. PERSONAL AUTHOR(S) Alford L. Ward	
13a. TYPE OF REPORT Interim 13b. TIME COVERED FROM Oct 84 TO Sep 85 14. DATE OF REPORT (Year, Month, Day) September 1987 15. PAGE COUNT 23	
16. SUPPLEMENTARY NOTATION AMS code: 612120.1400019; HDL project: 2E6725	

17. COSATI CODES			18. SUBJECT TERMS (Continue on reverse if necessary and identify by block number)
FIELD	GROUP	SUB-GROUP	
20	12		Computer calculations, limiter characteristics, silicon, forward bias, reverse switching, recombination lifetime, PIN diode, microwaves
09	03		

19. ABSTRACT (Continue on reverse if necessary and identify by block number)

Characteristics of microwave limiters, especially those of spike leakage and burnout, although little understood, are of great importance to the high-power microwave community. The Harry Diamond Laboratories computer program DIODE has been used to simulate limiter action. This is the first time the basic physical mechanisms of a limiter diode have been studied by a computer program. Simulations have included silicon PIN diode widths of from 0.5 to 10 μm, applied frequencies of 200 MHz to 50 GHz, and applied powers of 0.5 to 800 W. Illustrative carrier concentrations and electric fields are given as a function of distance across the diode and as a function of time, and diode and limiter output powers are given as a function of time. There is a frequency range where the limiter output power increases approximately linearly with frequency, which is the dependence predicted by linear theory. Avalanche breakdown during the reverse half-cycle is calculated for high-input powers. Limiter characteristics are shown to be strongly dependent upon diode temperature.

20. DISTRIBUTION / AVAILABILITY OF ABSTRACT ☒ UNCLASSIFIED/UNLIMITED ☐ SAME AS RPT. ☐ DTIC USERS	21. ABSTRACT SECURITY CLASSIFICATION UNCLASSIFIED
22a. NAME OF RESPONSIBLE INDIVIDUAL Alford L. Ward	22b. TELEPHONE (Include Area Code) (202) 394-3010 22c. OFFICE SYMBOL SLCHD-NW-RE

DD FORM 1473, 84 MAR 83 APR edition may be used until exhausted. All other editions are obsolete

SECURITY CLASSIFICATION OF THIS PAGE
UNCLASSIFIED

Foreword

This report was written in September 1985 as Part II of a report on limiters. Since Part I was never written, this part is now being published as originally written, except for the abstract and the first two paragraphs of the introduction, which have now been added. Therefore, this report does not benefit from information obtained by a later comparison between further calculations and laboratory measurements as had been reported at the High Power Microwave Technology for Defense Applications Conference, Kirkland Air Force Base, NM, 1–5 December 1986.

Contents

Figures

Figures (cont'd)

1. Introduction

Limiters are used to protect sensitive electronic components from damage by incident high-power microwave signals. Traditionally, gas tube limiters have been used for this purpose. However, gas tubes allow the transmission of an initial transient, spike leakage, of sufficient power to damage sensitive solid-state devices. Therefore, solid-state limiters have been introduced to remove the spike leakage from gas tubes and/or to protect semiconductors from moderate power microwaves.

The spike leakage from a gas tube limiter is understood to be a result of the time required to initiate an avalanche and to build up the gas tube arc. However, spike leakage may also be noted in solid-state limiters. This phenomenon in PIN diode limiters is not well understood. In particular, the parameters dictating spike leakage are not positively identified.

The Harry Diamond Laboratories (HDL) DIODE computer program, designed to study reverse-bias breakdown in semiconductors, has recently been used to study high-current characteristics of silicon PIN diodes at microwave frequencies [1]. It was reported that the forward turn-on transient caused the peak forward current to drop off linearly with frequency at high frequencies. This phenomenon is suggested as a possible physical model for spike leakage in PIN limiter diodes. This report gives the results of generic calculations to test this hypothesis. The greatest emphasis is upon the forward half-cycle of the applied sinusoidal voltage. Further cycles are calculated for a 1-μm intrinsic-width PIN diode. Some temperature effects are reported.

The computer program has been described in detail [2]. The circuit used for these calculations is shown in figure 1. Both the series resistor, R_s, and the load resistor, R_l, were set at 50 Ω for these calculations. The shunt capacitance was set at 2 pF for most calculations, but at 1 pF when indicated.

Although the computer program DIODE was designed to study reverse conduction only, it may calculate forward conduction also. However, only one polarity may be used per run, since calculations are halted for persistent negative fields. The field is considered positive for both polarities, and the doping profile is reversed in direction to change the polarity. Stored charges from the forward half-cycle may be used as initial conditions for the reverse half-cycle. Except in the case of avalanche breakdown, no stored charges are present at the end of the reverse half-cycle.

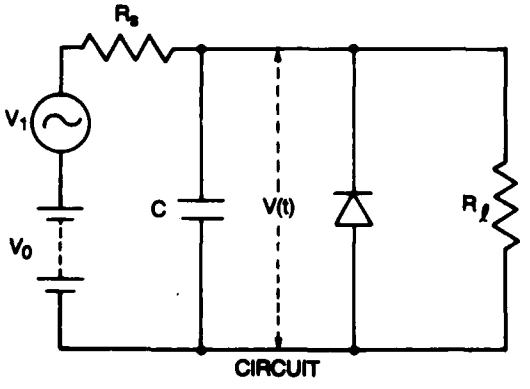

Figure 1. Circuit used for limiter calculations.

2. Forward Half-Cycle

Calculations of the forward turn-on transients for the PIN diode with constant applied voltages are helpful in preparation for calculating with sinusoidal voltages. For example, if the doping levels in the P and N regions are too low, the calculated current-voltage characteristic is abnormal. On the other hand, if the levels are too high, calculation instability will be noted more readily in the step voltage calculation.

The 10-V forward turn-on transient for a 5-μm PIN diode is shown in figure 2. The diode area is 5×10^{-4} cm^2. It is seen that the diode voltage peaks at about 2 V at about 70 ps and reaches a quasi-equilibrium value of 0.7 V at 2 ns. The current through the load resistance behaves similarly, but the current through the diode is still increasing slowly at 2 ns. The carrier distributions across the diode are shown in figure 3 for the turn-on transient of figure 2. It is seen that the maximum voltage occurs shortly after the electron and hole distributions overlap. The voltage buildup is determined by the external circuit resistance-capacitance (RC) time constant, 0.1 ns. The drop in voltage is

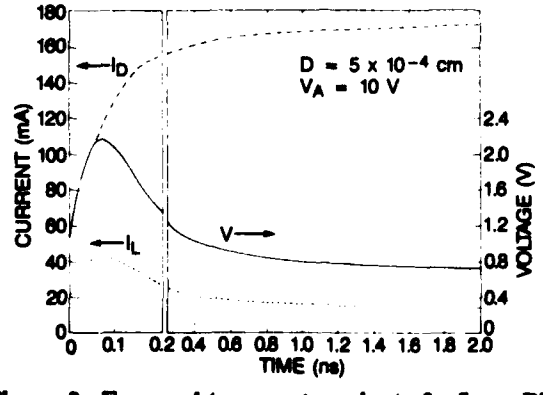

Figure 2. Forward turn-on transient of a 5-μm PIN diode. Diode current is I_D and load current is I_L. First 0.2 nanosecond is shown on an expanded time scale.

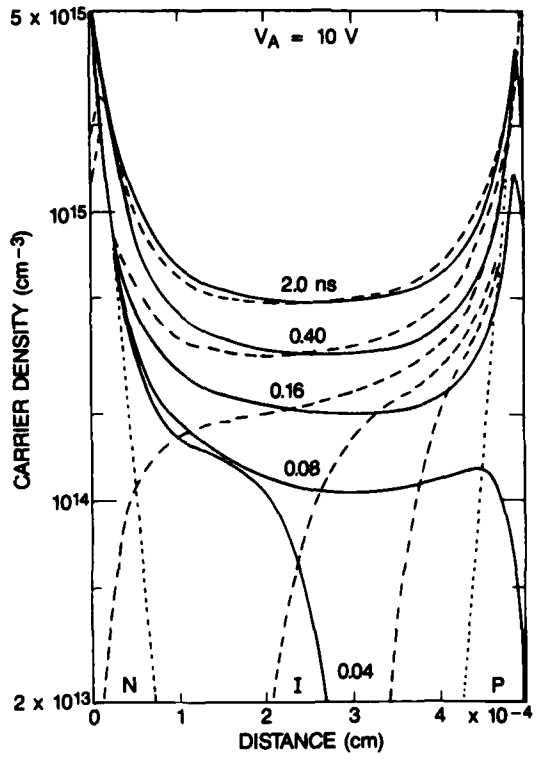

Figure 3. Carrier distributions for turn-on transient of figure 2. Electron distributions are shown as solid lines, hole distribution as dashed lines, and doping profile as dotted lines. Parameter is time in nanoseconds.

due to the increasing conductance in the intrinsic region. The slow buildup of carriers in the intrinsic region after 0.4 ns is largely determined by the buildup of charges in the P and N regions. Further discussion may be found in another work [2]. The electric field distributions corresponding to the carrier distributions shown in figure 3 are shown in figure 4. The doping profiles in the P and N regions are chosen so that E extrapolates approximately to zero at the calculation boundaries. In actuality, negative or reverse fields occur in the P and N regions so that the diffusion current is reduced to that which is conducted across the intrinsic region. This negative voltage, called the built-in voltage for zero current, is reduced as the current increases. No attempt is made to cor-

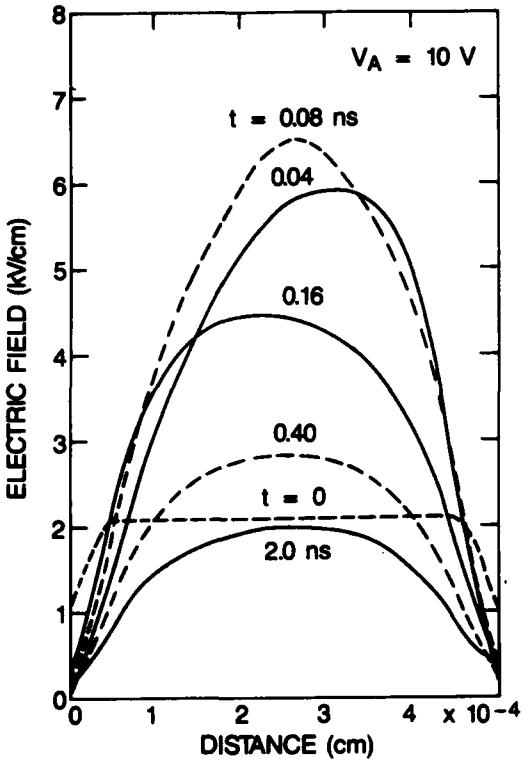

Figure 4. Field distributions for turn-on transient of figure 2. Dashed and solid lines are used for clarity. Parameter is time in nanoseconds.

rect for these negative voltage components in these calculations.

The instantaneous power through the diode or the load is the product of the diode voltage and the appropriate current. For sinusoidal waveforms, the maximum power through the load is given by $V^2/4R$, and the average power is one-half the maximum. When the waveform is not sinusoidal, the factor of one-half is usually not valid. Therefore, the peak powers will be used in this report. The power through the load is designated the limiter output power. The variation of the output power as a function of time for the diode of figure 2 is shown in figure 5 as the dashed curve. Also shown in figure 5 are portions of the forward half sine waves at various frequencies. It is seen that the limiter output power is not sinusoidal,

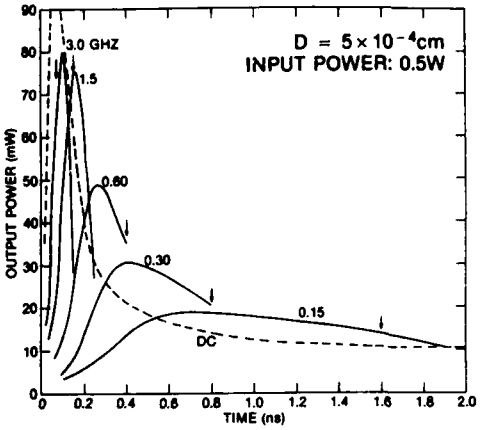

Figure 5. Output power as a function of time for diode of figure 2. Parameter is frequency in gigahertz. Vertical arrows denote time of applied voltage maximum.

especially for the lower frequencies. The peak output powers are seen to increase with frequency, having an envelope which is similar (on the time scale) to the dc turn-on transient. At higher frequencies, the peak power decreases due to the RC time constant for the external circuit, 0.1 ns for these calculations. The vertical arrows indicate the time of the maximum applied voltage. Calculations for the lower frequencies were truncated short of one-half period to reduce costs.

The peak powers from figure 5 are plotted in figure 6 as a function of frequency. Similar data for higher applied voltages are also plotted in figure 6. The parameter in this figure is the peak instantaneous input power. These calculations were made with a recombination lifetime of 50 μs. This lifetime refers to low currents in intrinsic material. For the high currents considered here, the effective lifetime is much shorter. Calculations were made with lifetimes doubled and also halved. The results are shown by the dashed curves. Shorter lifetimes (higher recombination) reduce the current, and therefore the power is reduced approximately in proportion to the current. Thus the lowest frequency for which a variation of the lifetime has no

effect on the peak limiter power increases as the input power increases. This lowest frequency is also a function of diode width. The straight dashed line in figure 6 indicates the variation of limiter output for a 5-μm diode derived from the low-level linear theory [3,4]. No variation with input power was given. The present computed curves are seen to have regions where the output power increases roughly linearly with frequency as in the linear theory. The intersection of the dashed curve with the 10-mW output axis, considered the ideal limiter output, was postulated to give the frequency above which spike leakage was present. The relation of the present calculations to spike leakage will be discussed below.

Some of the data of figure 6 have been replotted in figure 7 as a function of input power, with frequency as a parameter. This

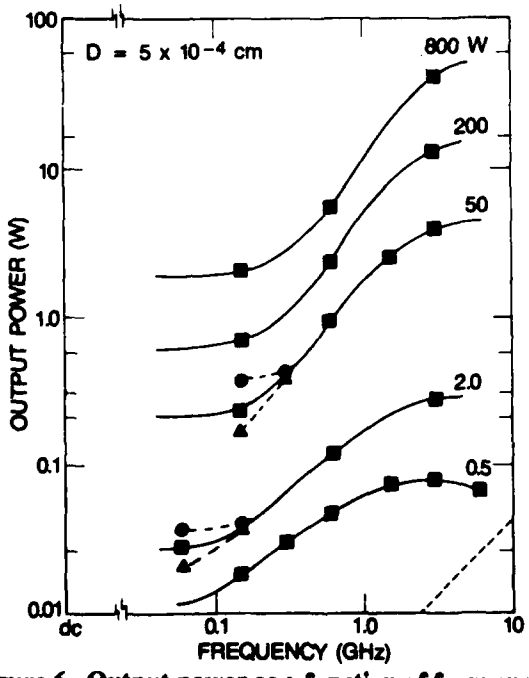

Figure 6. Output power as a function of frequency, with input power in watts as parameter. Points on dashed curves are for different recombination lifetimes. Straight dashed line at lower right is from low-level linear theory.

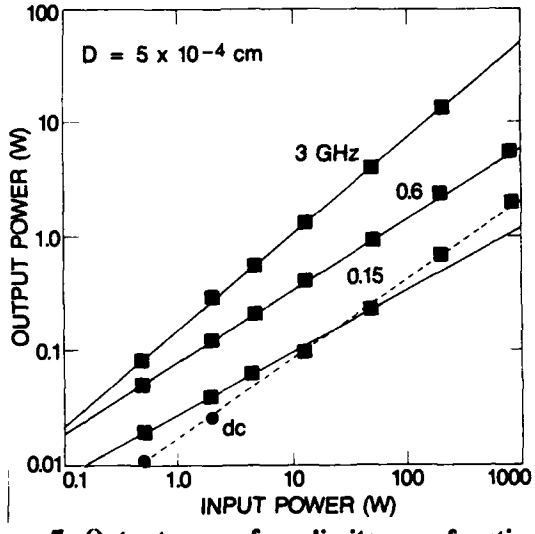

Figure 7. Output power from limiter as a function of input power. Parameter is frequency in gigahertz.

mode of plotting is more suitable for comparison with experimental measurements where the frequency is fixed and the input power is varied. The amount of isolation may be determined directly from figure 7. For example, for 10-W input power the isolation is just over 20 dB for lower frequencies, but drops to about 10 dB at 3 GHz. The slope of the 3-GHz line is greater than one, indicating a decrease in isolation with input power; but at lower frequencies, the slope is less than one, indicating an increase in isolation with input power. Two points are shown for the dc peak power. At higher powers the dc data merge with the 0.15-GHz curve, the latter of which changes slope to agree with the dc slope.

Calculations have also been made of the forward trar.sients for various other diode widths with dc and various frequencies applied. The results for a nearly constant input power are given in figure 8. The input power was 50 W for all thicknesses except for the 2.5-μm diode, where the input power was 40 W. It is seen that each curve has a region of approximately linear variation of peak power with

frequency. If these portions of the curves are extrapolated to a fixed power, the intercept varies with the square of the frequency. This is in agreement with the linear theory [3,4]. The area of each diode was assumed to be numerically equal to the diode width, where the units are in centimeters; i.e., the 5-μm diode had an area of 5×10^{-4} cm^2. Therefore all diodes had the same depletion capacitance, approximately 1 pF. Calculations with different areas yield different results, since some processes are functions of current densities, whereas others depend on the total current. The calculations for the 0.5-μm diode were made with a shunt capacitance of 1 pF; all others, with 2 pF. This lower capacitance increases the frequency at which the peak power decreases with frequency. The calculated falloffs in power for the capacitances used have a slope of –2 on this plot and form asymptotes to the calculated curves.

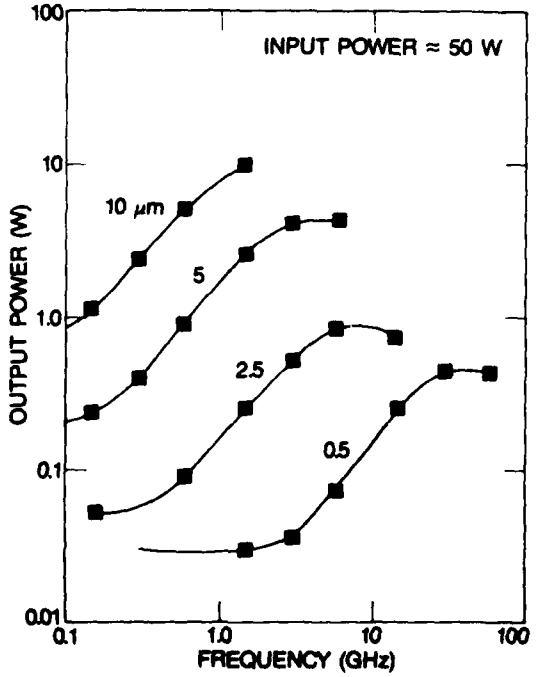

Figure 8. Output power for various diode widths, given in micrometers. Input power is 50 W for each diode thickness except 2.5-μm diode, where input power is 40 W.

3. One Full Cycle

The stored charges in the diode at the end of the forward half-cycle are used as the initial condition for calculations of the following reverse-biased half-cycle. A diode width of 1 μm was chosen to make an extensive series of full-cycle calculations. This diode has a reverse breakdown of 35 V. Based on the results of figure 8, three frequencies were chosen: 5, 10, and 20 GHz. Also, three voltage amplitudes were chosen: 100, 200, and 400 V, corresponding to average input powers of 25, 100, and 400 W. For 100 V applied, the stored charge in the intrinsic region was within 10 percent of 1×10^{16} cm^{-3} for all three frequencies. The charges in the P and N regions varied much more; more charge was stored at the lower frequencies. At the higher applied voltages, the stored charges varied as much as 25 percent with frequency. This variance notwithstanding, it was decided to save time and use an average distribution for each applied voltage.

An example for a full-cycle calculation is given in figure 9. The applied voltage amplitude is 100 V and the frequency is 10 GHz. At room temperature, the forward diode voltage is about 2.5 V while the reverse peak is about 12 V. Defining the percentage rectification as $[1 - V_f/V_r] \times 100$, where V_f is the peak forward voltage and V_r is the reverse peak voltage, one gets the ratio of 79 percent. The stored charge in the N region is collected in about 10 ps, and the reverse voltage starts to increase at that time. For a fuller discussion, see the section on reverse switching transients given in another work [2]. Although the applied voltage crosses the zero axis at 100 ps, the diode voltage lags very nearly a full quarter cycle. All stored charges were collected during the reverse half-cycle for all calculations, except in the case of reverse breakdown.

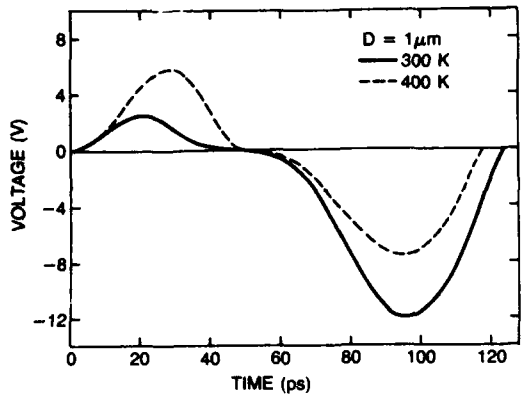

Figure 9. Voltage as a function of time for 1-μm diode at 10 GHz. Applied voltage amplitude is 100 V.

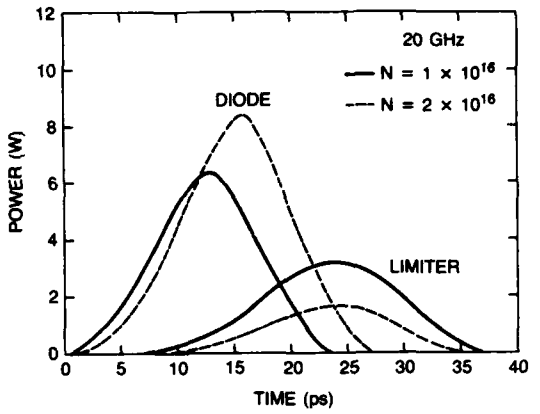

Figure 10. Effect of initial stored charge on reverse power for 1-μm diode. Solid lines apply to stored carrier densities of 1×10^{16} cm^{-3} in the intrinsic region; dashed lines for 2×10^{16} cm^{-3}. Power dissipated by the diode is labeled "DIODE" whereas power dissipated by the load is labeled "LIMITER" output.

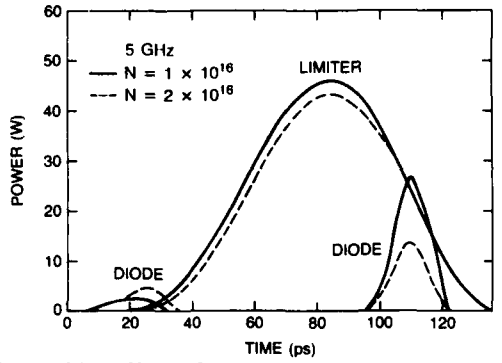

Figure 11. Effect of stored charge on reverse power at 5 GHz, in 1-μm diode. Second power peak (at about 100 ps) of diode power is result of avalanching.

To test the magnitude of the effect of the amount of stored charge used in the reverse half-cycle, calculations were made with half the indicated stored charge. The results for a 20-GHz calculation with an applied voltage of amplitude of 200 V (100 W) is shown in figure 10. Only the reverse half-cycle is shown. The forward half-cycle results in a stored carrier density level of 2×10^{16} cm^{-3}. The lower stored charge lowers the current in the diode and allows a higher voltage to develop across the diode, thus increasing the limiter output power. A similar plot of diode and limiter power is shown in figure 11 for a frequency of 5 GHz. The 1-μm diode is seen to be a peak limiter for the reverse half-cycle at 5 GHz. At this frequency, the variation in the initial stored charge level is seen to have a very small effect on the power through the limiter. This is considered partial justification for not changing the initial charge distributions as a function of frequency. The power in the diode due to the stored charges disappears in about 30 ps, but the reverse bias reaches a maximum of about 47 V, 12 V above the dc breakdown level, and avalanche current appears just before 100 ps.

Calculations were also made of the reverse half-cycle with no stored charge, as would be the case for an initial negative applied voltage. Generally, the results differed little from those calculated with the stored charge at 5 GHz, but the difference increased at the higher frequencies. An exception is the case where the voltage is near the avalanche breakdown threshold, where a small voltage change causes a large current change.

The peak power transmitted by the limiter as a function of frequency is shown in figure 12

for the three input power levels used. The input power levels, indicated as parameters, are average powers. The limiter becomes less effective at higher frequencies for the forward half-cycle, but more effective during the reverse half-cycle. As the frequency increases, the maximum voltage across the diode approaches the same value during the forward and reverse half-cycles; i.e., there is no rectification. The peak power dissipated by the diode is shown as a function of frequency in figure 13. The power increases as a function of frequency during both the forward and reverse half-cycles. However, at higher frequencies, one would expect the power in each bias direction to decrease with frequency. The sums of the peak powers dissipated in the diode, figure 13, and transmitted by the limiter, figure 12, are far less than the average input power for both the forward and reverse half-cycles. It is assumed that the unaccounted power would be reflected by the limiter back to the power source.

4. A Growing Sinusoidal Waveform

Only with a computer can one apply a large microwave signal with virtually no rise time. In the real world, any microwave signal will require a number of full periods to reach a constant amplitude. The method of using stored charges from a forward half-cycle to compute the power in the reverse half-cycle allows one to simulate a growing applied voltage to the diode. The input amplitude may be increased only at the forward-to-reverse transition, since the diode voltage lags the applied voltage in the reverse-to-forward transition.

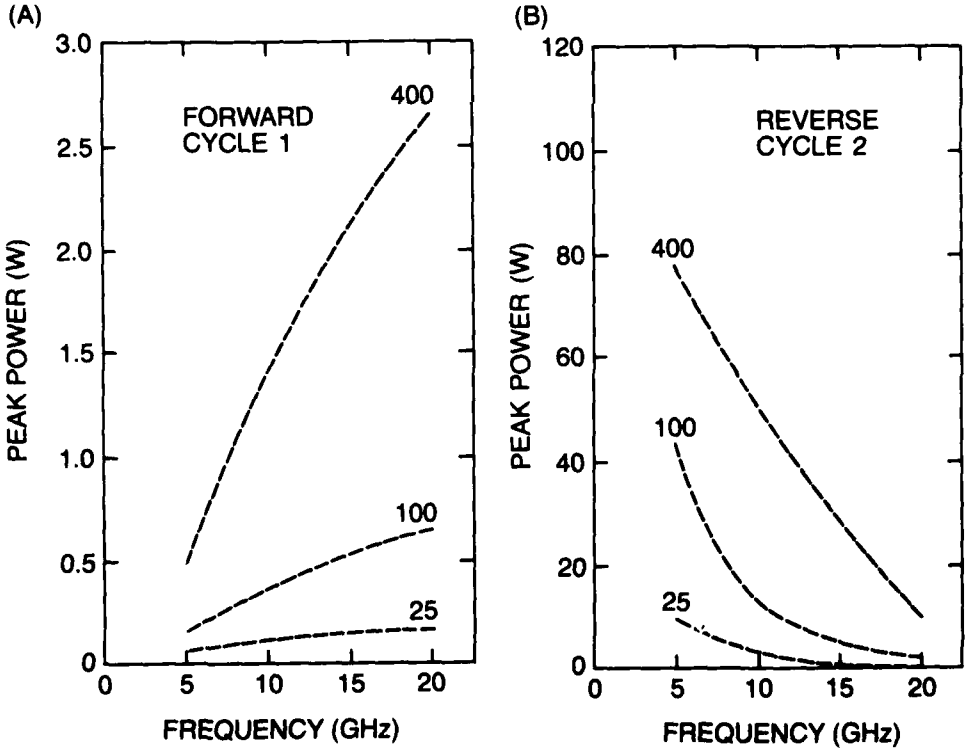

Figure 12. Power dissipated in load as a function of frequency for three average input powers in watts as indicated for a 1-μm diode: (a) initial forward half-cycle and (b) following reverse half-cycle.

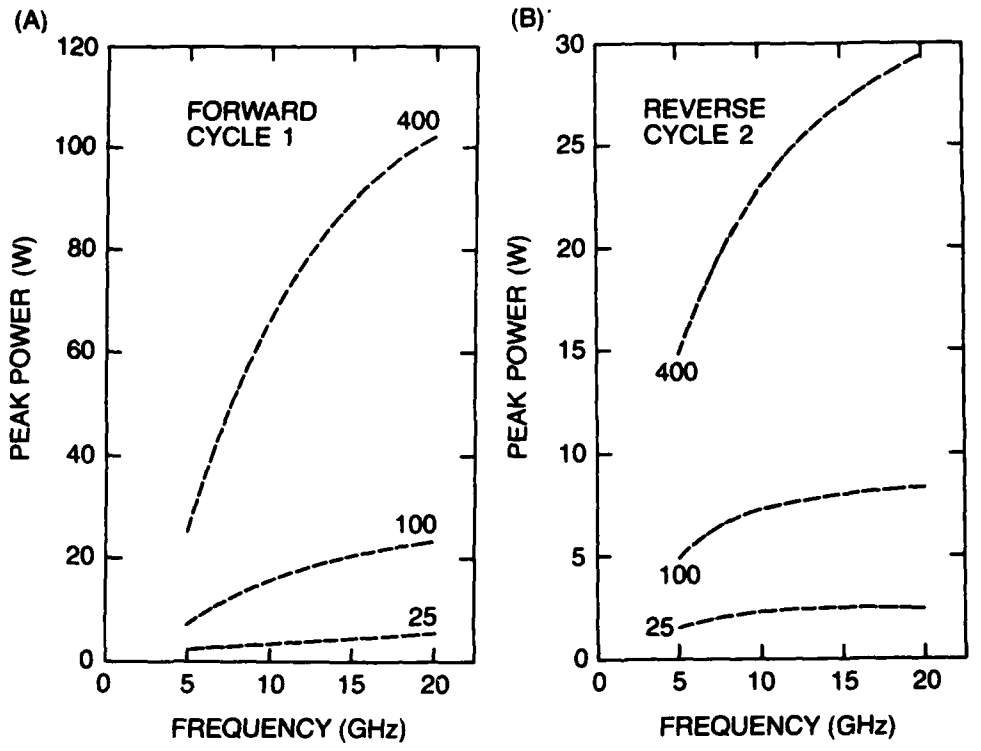

Figure 13. Power dissipated in 1-μm diode as a function of frequency for three average input powers in watts: (a) initial forward half-cycle and (b) following reverse half-cycle.

A series of calculations with increasing input voltage amplitudes was made for a 1-μm diode at 10 GHz. The first half-cycle had a voltage amplitude of 100 V, the next full cycle was at 200 V, and the following full cycle at 400 V, as shown in figure 14. The diode voltage waveform is similar to that shown previously for the first three half-cycles. However, during the second reverse half-cycle, the reverse breakdown voltage is exceeded and avalanching occurs. This current is sufficient to drop the diode voltage to zero before these carriers could be removed from the diode by recombination and carrier transport. These stored charges were used as initial conditions for the third forward half-cycle. These stored charges reduced the resistivity of the intrinsic region. The maximum voltage for this cycle barely exceeded that for the first forward half-cycle, with 100 V applied rather than 400 V. The voltage peak was 2.5 V with the stored charge, as compared to 8.2 V calculated without the stored charge. The power from the limiter is proportional to the square of the voltage. Avalanching and its stored charges may play a part in the termination of spike leakage. The corresponding power through the diode and the output from the limiter are shown in figure 15 for the growing voltage calculations. The diode power during avalanche reached 1 kW, but the FWHP (full width half power) was only about 4 ps.

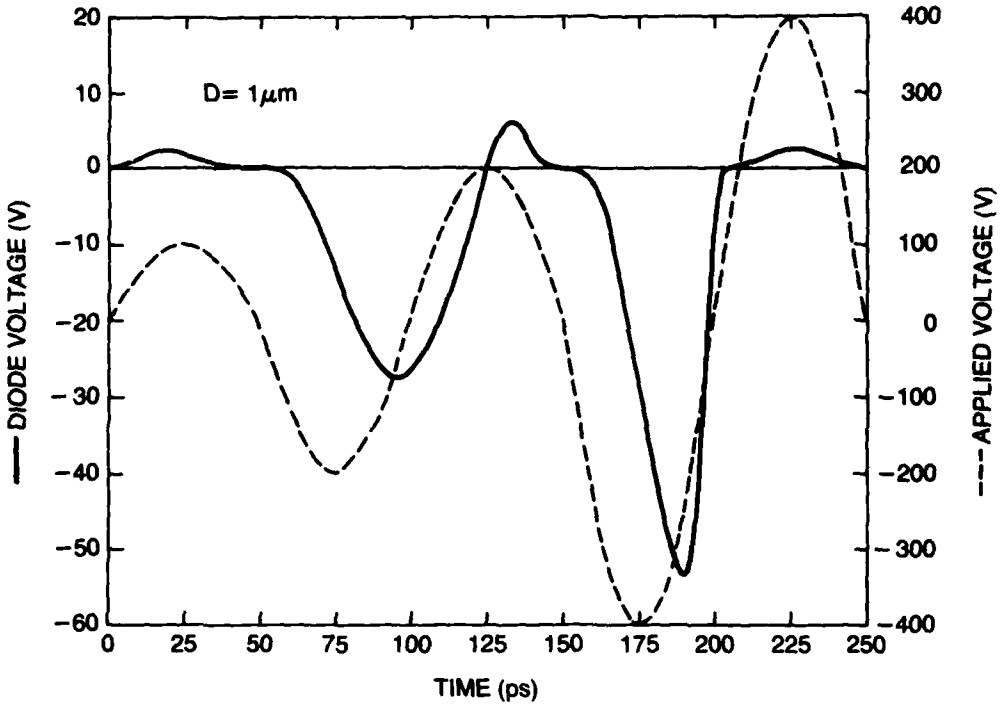

Figure 14. Diode voltage for a growing input voltage waveform. Dashed line and right scale show applied waveform.

5. Temperature Effects

All the calculations reported in the preceding sections were made for the diode at room temperature, 300 K. A few runs were made with the temperature increasing as a function of the power dissipated. For example, for the 1-μm diode, with an amplitude of 400 V and a frequency of 10 GHz, the temperature was found to increase only 62 mK during the first forward half-cycle. This voltage is just sufficient to cause avalanching at this frequency, as was seen in figures 14 and 15. Without avalanche, the temperature increase in the reverse half-cycle is about one-half that for the forward half-cycle. Thus the full cycle for the above conditions has a temperature increase of about 0.1 K in 0.1 ns. Thus, neglecting heat flow, it would take 0.3 μs to increase the tem-

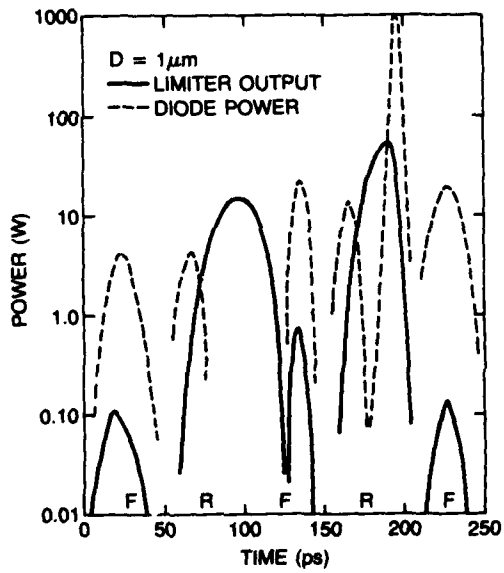

Figure 15. Diode and limiter power for growing input voltage waveform of figure 14. Forward and reverse biases are indicated by F and R, respectively, at bottom of figure.

perature by 300 K, a temperature rise which will usually lead to burnout [2]. One concludes that reverse breakdown may be a cause of limiter burnout at times shorter than 1 μs.

The temperature distribution across the intrinisic region is parabolic after the forward half-cycle, similar to the field distributions shown in figure 4. The distribution of the increase in temperature peaks in the P and N regions for the reverse half-cycle; an example is given in figure 17 of another report [1]. The temperature after the full cycle is then roughly constant.

Calculations have also been made for a constant temperature of 400 K. The diode voltage as a function of time at 400 K for the 1-μm diode at 10 GHz is also shown in figure 9. The forward voltage is seen to increase with temperature, whereas the reverse voltage decreases with temperature. The dominant cause for these changes is the decrease in mobility of the charge carriers with temperature. Thus it takes longer both to fill and to remove the charges from the intrinsic region. The former effect is to increase the resistivity and voltage during turn-on, and the latter effect is to decrease the resistivity and voltage during turn-off. This diode is seen to be a poorer rectifier at the higher temperature. The powers transmitted by the limiter for the two temperatures are shown in figure 16. The reduction of transmitted power in the reverse direction at 400 K more than compensates for the increase during forward conduction. The power dissipated in the diode is shown in figure 17 at 300 and 400 K. In this case the power increases with temperature for both bias directions, but the proportional increase is much greater in the forward direction. This is largely due to the decreasing effect of recombination during forward bias as the temperature increases. The temperature effects are quite large and must be included in high power calculations.

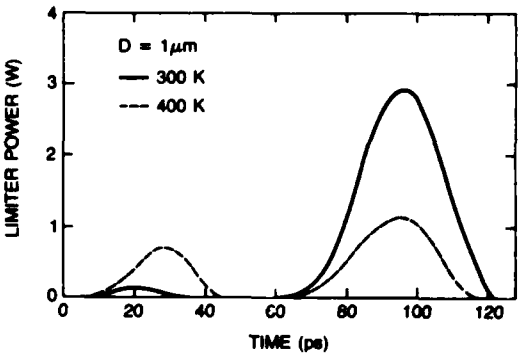

Figure 16. Transmitted limiter power at 300 and 400 K as a function of time at 10 GHz.

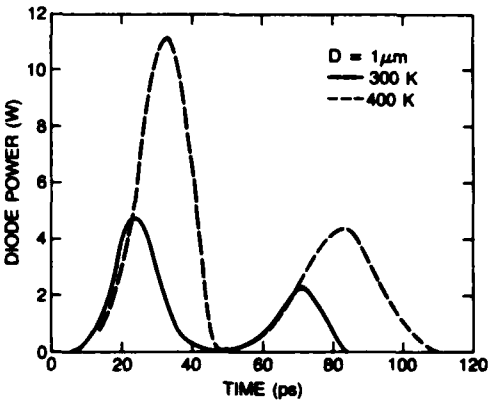

Figure 17. Dissipated diode power as a function of time at 10 GHz and at 300 and 400 K.

6. Discussion

The extensive calculations discussed in the preceding sections show some promise in increasing the understanding of limiter action and the problem of spike leakage. At present, further progress from calculations is hampered mainly by the lack of well-documented experimental data. Only one measured value has been published [3] for the limiter power at one frequency which agrees with the linear theory of Leenov [4]. As shown in figure 6, our calculations show an increase in limiter power with

frequency at more than an order of magnitude lower frequency than the linear theory. This is hard to understand since most comparisons of results from the DIODE computer program show deviations from experimental measurements in the opposite direction. For example, Caulton et al [5] measured the frequency at which rectification disappears in PIN diodes of from about 100- to 300-μm width. Our calculations were made for PIN diodes of from 1- to 50-μm widths, which, when extrapolated, show the disappearance of rectification at much higher frequencies than reported by Caulton. Also, unpublished measurements in our laboratory of turn-on and turn-off transients of diodes show much longer time scales than are calculated by the DIODE program. This time difference has been tentatively explained by the use of ideal (higher) carrier mobilities in calculations and by long rise times seen in experimental input voltages.

At present, the most plausible explanation for the lower calculated frequency for limiter power increase is that the initial transient which is calculated pertains to the higher power spike leakage, whereas the experimental measurement pertains to the lower power equilibrium condition. Turn-on and turn-off as well as limiter measurements, made for the same well-documented diodes, will be necessary to resolve this question.

Literature Cited

1. A. L. Ward, *Calculations of High-Current Characteristics of Silicon Diodes at Microwave Frequencies*, Harry Diamond Laboratories, HDL-TR-2057 (October 1984).

2. A. L. Ward, *Calculations of Second Breakdown in Silicon*, Harry Diamond Laboratories, HDL-TR-1978 (August 1982).

3. N. J. Brown, *Design Concepts for High-Power PIN Diode Limiting*, IEEE Trans. Microwave Theory Tech., *MTT-15* (1967), 732-742.

4. D. Leenov, *The Silicon PIN Diode as a Microwave Radar Protector at Megawatt Levels*, IEEE Trans. Electron Devices, *ED-11* (1964), 53-61.

5. M. Caulton, A. Rosen, P. J. Stable, and A. Gombar, *PIN Diodes for Low-Frequency High Power Switching Applications*, IEEE Trans. Microwave Theory Tech., *MTT-30* (1982), 875-882.

DISTRIBUTION

ADMINISTRATOR
DEFENSE TECHNICAL INFORMATION CENTER
ATTN DTIC-DDA (12 COPIES)
CAMERON STATION, BUILDING 5
ALEXANDRIA, VA 22314

COMMANDER
US ARMY MATERIEL COMMAND
ATTN AMCLD
5001 EISENHOWER AVE
ALEXANDRIA, VA 22333-0001

DEFENSE ADVANCED RESEARCH
PROJECT AGENCY
ATTN LTC RICHARD L. GULLICKSON, DEO
1400 WILSON BLVD
ARLINGTON, VA 22209

DEFENSE COMMUNICATIONS AGENCY
ATTN DR. PRAVIN JAIN
8TH STREET & SOUTH COURTHOUSE RD
ARLINGTON, VA 22204

DEFENSE INTELLIGENCE AGENCY
ATTN D. SPOHN, DB-4C2
ATTN DR. JAMES COLEMAN, DT-4C
ATTN CPT ROGER J. HOFFMAN, DC-7B
WASHINGTON, DC 20301

DIRECTOR
DEFENSE NUCLEAR AGENCY
ATTN CPT STONE, RAEE
ATTN GORDON SOPER
ATTN JACK MANSFIELD
WASHINGTON, DC 20305

INSTITUTE FOR DEFENSE ANALYSIS
ATTN DR. DEBORAH LEVIN
1801 N BEAUREGARD STREET
ALEXANDRIA, VA 22311

ASSISTANT TO THE SECRETARY OF DEFENSE
(ATOMIC ENERGY)
ATTN DR. RICHARD L. WAGNER
THE PENTAGON
ROOM 3E1074
WASHINGTON, DC 20301-3050

COMMANDER
US ARMY ARMAMENT, MUNITIONS, & CHEMICAL
COMMAND
ATTN DRSMC-LEP-L, TECHNICAL LIBRARY
ATTN DRSMC-ASF, FUZE & MUNITIONS
SUPPORT DIV
ROCK ISLAND, IL 61299

DIRECTOR
US ARMY BALLISTIC RESEARCH
LABORATORY
ATTN DRDAR-TSB-S (STINFO)

DIRECTOR
US ARMY BALLISTIC RESEARCH
LABORATORY (cont'd)
ATTN DRSMC-BLV-R (A), J. McNEILLY
ATTN DRSMC-BLV-A (A), M. VOGEL
ABERDEEN PROVING GROUND, MD 21005

COMMANDER
US ARMY CAORA
ATTN ATOR-CAS-SO, MR. WALTERS
ATTN ATOR-CAS-SO, MR. HANSEN
FT LEAVENWORTH, KS 66027

US ARMY COMBINED ARMS CENTER
ATTN ATZL-CAM-D, A. T. BOWEN
FT LEAVENWORTH, KS 66027

COMMANDER
USA AIR DEFENSE SCHOOL
ATTN ATSA-CDM-W, CPT RAY GERTMAN
FT BLISS, TX 79916

US ARMY ELECTRONICS TECHNOLOGY &
DEVICES LABORATORY
ATTN DELET-MW, MR. WILSON,
EVANS AREA
ATTN DELET-DD
FT MONMOUTH, NJ 07703

COMMANDER
US ARMY ELECTRONIC WARFARE LABORATORY
OFFICE OF MISSILE ELECTRONIC WARFARE
ATTN DELEW-M-TAC, D. ALVAREZ,
A. K. PATTNI
WHITE SANDS MISSILE RANGE, NM 88002

COMMANDER
US ARMY FOREIGN SCIENCE
& TECHNOLOGY CENTER
ATTN DRXST-SD1, DR. T. A. CALDWELL
220 SEVENTH STREET, NE
CHARLOTTESVILLE, VA 22901

US ARMY MATERIEL SYSTEMS ANALYSIS ACTIVITY
ATTN DRXSY-MP
ATTN DRXSY-CS, B. BRADLEY
ATTN DRXSY-GC, JAMES C. LIU
ABERDEEN PROVING GROUND, MD 21005-5071

COMMANDER
US ARMY MISSILE COMMAND
ATTN DRSMI-RHB, H. GREENE
ATTN DRSMI-YSO, L. ALTGILBERS
REDSTONE ARSENAL, AL 35809

COMMANDER
US ARMY MISSILE & MUNITIONS
CENTER & SCHOOL
ATTN ATSK-CTD-F
REDSTONE ARSENAL, AL 35809

DISTRIBUTION (cont'd)

US ARMY BELVOIR RD&E CENTER
ATTN STRBE-F
ATTN STRBE-FG
FT BELVOIR, VA 22060

DOD
PM MOBILE ELECTRIC POWER
ATTN AMC-PM-MEP-T
7500 BACKLICK ROAD
BUILDING 2089
SPRINGFIELD, VA 22150-3107

COMMANDER
US ARMY ENGINEER SCHOOL
ATTN ATZA-TSM-G
FT BELVOIR, VA 22060-5249

US ARMY RESEARCH OFFICE
PO BOX 12211
ATTN DRXRO-PH, DR. B. D. GUENTHER
RESEARCH TRIANGLE PARK, NC 27709

COMMANDER
US ARMY TRAINING & DOCTRINE COMMAND
ATTN ATDO-TAG, WOLFORD
ATTN ATCD-M, GRAY
FT MONROE, VA 23651

DEPARTMENT OF THE ARMY
DEPUTY CHIEF OF STAFF, RDA
WASHINGTON, DC 20310

HQ, AMC
ASSISTANT DEPUTY FOR SCIENCE & TECHNOLOGY
ATTN DR. R. L. HALEY, AMCDRA-ST
5001 EISENHOWER AVENUE
ALEXANDRIA, VA 22333-0001

INDUSTRIAL COLLEGE OF THE ARMED FORCES
ATTN ICFA-MSM, ROGER LEWIS
FT L. J. McNAIR
WASHINGTON, DC 20319

LETTERMAN ARMY INSTITUTE OF RESEARCH
ATTN SGRD-ULZ-IR, MAJ VANDRE
PRESIDIO OF SAN FRANCISCO, CA 94129

AIR FORCE WEAPONS LABORATORY
ATTN DR. BABU SINGARAJU, AFWL/NTC
ATTN MR. OTIS A. DAVENPORT, AFWL/NTC
KIRTLAND AFB, NM 87117

COMBAT DATA INFORMATION CENTER
AFWL-FIESD (CDIC)
WRIGHT-PATTERSON AFB, OH 45433

ROME AIR DEVELOPMENT CENTER
ATTN MR. RICHARD RABE, RADC/RBCM
GRIFFIS AFB, NY 13441

WRIGHT AERONAUTICAL LABORATORY
ATTN ROLAND D. VON ROHR, AAWW-1
ATTN DR. EDWIN B. CHAMPAGNE, AFWL/AAD
WRIGHT-PATTERSON AFB, OH 45433

HQ, USAF
DEPARTMENT OF THE AIR FORCE
ATTN MAJ CLARENCE M. BOSE, INYX
WASHINGTON, DC 20330

US AIR FORCE TECHNICAL
ASSESSMENT CENTER
ATTN CPT ROSS L. AMICO, TAO
PATRICK AFB, FL 32925

HQ, USAF/SAMI
WASHINGTON, DC 20330

RELIABILITY ANALYSIS CENTER
RADC (RBRAC)
ATTN DATA COORDINATOR/GOVT PROGRAMS
GRIFFISS AFB, NY 13441

HQ
AIR FORCE ELECTRONIC WARFARE
CENTER (ESC)
ATTN SAXA, J. GIORLANDO
SAN ANTONIO, TX 78243

HEADQUARTERS, AIR FORCE SYSTEMS
COMMAND
ATTN DLWM, CPT JUDITH COOK
ANDREWS AFB, MD 20334

USAFSAM/RZP
ATTN DAVID N. ERWIN
BROOKS AFB, TX 78235

AFWAL/AADM
ATTN DONALD REES
WRIGHT-PATTERSON AFB, OH 45433

NAVAL INTELLIGENCE SUPPORT
CENTER
ATTN ARTHUR G. COBLEIGH, JR., NISC-51
ATTN MR. ALBERT LEAVITT
4201 SUITLAND ROAD
WASHINGTON, DC 20390

NAVAL RESEARCH LABORATORY
ATTN MOSHE FRIEDMAN, CO 4700.1
ATTN SIDNEY L. OSSAKOW, CO 4700
ATTN T. J. WIETING, CO 6652
4555 OVERLOOK AVENUE, SW
WASHINGTON, DC 20376

DISTRIBUTION (cont'd)

NAVAL SEA SYSTEMS COMMAND
ATTN GEORGE M. BATES
PMS-405-300
WASHINGTON, DC 20362

COMMANDER
NAVAL SURFACE WEAPONS CENTER
ATTN DR. VINCENT PUGLIELLI, R. RICHARDSON
DAHLGREN, VA 22448

AAI CORPORATION
PO BOX 6767
RECORDS DEPARTMENT
BALTIMORE, MD 21204

ALPHA INDUSTRIES, INC
SEMICONDUCTOR DIVISION
ATTN WILLIAM ZETTLER
20 SYLVAN ROAD
WOBURN, MA 01801

ANALYTICAL SYSTEMS ENGINEERING CORP
OLD CONCORD ROAD
ATTN LIBRARIAN
BURLINGTON, MA 01803

ARNOLD ENGINEERING DEVELOPMENT
CENTER
ATTN LARRY CHRISTENSEN
MAIL STOP 640
TULLAHOMA, TN 37388

BERKELEY RESEARCH ASSOCIATES
PO BOX 852
ATTN DR. E. C. ALCARAZ
SPRINGFIELD, VA 22150

THE BDM CORPORATION
ATTN MR. IGOR D. GERHARDT
2227 DRAKE AVENUE
SUITE 25
HUNTSVILLE, AL 35805

BOEING MILITARY AIRPLANE COMPANY
ATTN CLETUS SUTTER
M/S: K75-50
3801 SOUTH OLIVER
WICHITA, KS 67210

BOEING AEROSPACE COMPANY
PO BOX 3707
ATTN D. W. EGELKROUT, MS 2R 00
SEATTLE, WA 98124

BOEING AEROSPACE COMPANY
PO BOX 3999
ATTN DR. ERVIN J. NALOS, 2-3741-EJN-288
SEATTLE, WA 98124

DIRECTED TECHNOLOGIES, INC
ATTN MR. IRA F. KUHN, JR.
1226 POTOMAC SCHOOL ROAD
McLEAN, VA 22101

DIRECTOR
NATIONAL SECURITY AGENCY
ATTN MS GAIL J. REINHEIMER, A4
FT MEADE, MD 20755

EOS TECHNOLOGIES, INC
ATTN DR. R. E. LeLEVIER
606 WILSHIRE BLVD
SUITE 700
SANTA MONICA, CA 90401

ENGINEERING SOCIETIES LIBRARY
ATTN ACQUISITIONS DEPARTMENT
345 EAST 47TH STREET
NEW YORK, NY 10017

GENERAL DYNAMICS/POMONA DIVISION
ATTN DR. K. H. BROWN, MZ 401-10
ATTN DIVISION LIBRARY, 4-20
ATTN MR. HAME, MZ 401-11
POMONA, CA 91769

GRUMMAN AEROSPACE CORPORATION
ATTN A. G. ZIMBALATTI
BETHPAGE, NY 11714

R. C. HANSEN, INC
PO BOX 215
ATTN R. C. HANSEN
TARZANA, CA 91356

IRT CORPORATION
ATTN HAROLD T. BUSCHER
3030 CALLAN ROAD
SAN DIEGO, CA 92121

IRT CORPORATION
PO BOX 85317
ATTN DR. FRANK CHILTON
SAN DIEGO, CA 92138

KAMAN SCIENCES CORPORATION
ATTN EDWARD E. CONRAD, DOC CONT
ATTN SUITE 1200
1911 JEFFERSON DAVIS HIGHWAY
ARLINGTON, VA 22202

DASIAC-DETIR
KAMAN TEMPO
ATTN MR. F. WIMENITZ
2560 HUNTINGTON AVENUE, SUITE 500
ALEXANDRIA, VA 22303

DISTRIBUTION (cont'd)

KAMAN TEMPO
ATTN D. REITZ
816 STATE STREET
(PO DRAWER QQ)
SANTA BARBARA, CA 93102

LAWRENCE LIVERMORE NATIONAL
LABORATORY
PO BOX 808
ATTN MR. BLAND, L-153
ATTN HRIAR S. CABAYAN, L-313
ATTN J. B. CHASE, L-313
ATTN T. R. KONCHER, L-389
ATTN GEORGE H. MILLER, L-13
ATTN W. J. SHOTS, L-23
ATTN WALTER R. SOOY, L-488
LIVERMORE, CA 94550

LOCKHEED MISSILES & SPACE
COMPANY, INC
ATTN JOHN G. SIAMBIS
3251 HANOVER STREET
PALO ALTO, CA 94304

LOS ALAMOS NATIONAL LAB
PO BOX 1663 MS-5000
ATTN R. S. DINGUS
ATTN ROBERT F. HOBERLING
ATTN JEREMY A. LANDT
ATTN FREDERICK A. MORSE
ATTN J. W. TAYLOR
ATTN L. B. WARNER
LOS ALAMOS, NM 87545

MARTIN MARIETTA ORLANDO
AEROSPACE
PO BOX 5837, MP 480
ATTN DR. B. L. CLARK
ATTN MR. CHARLES R. CRANFORT
SAND LAKE ROAD
ORLANDO, FL 32855

MAXWELL LABORATORIES, INC
ATTN F. MARC de PIOLENC
8835 BALBOA AVENUE
SAN DIEGO, CA 92123

McDONNELL DOUGLAS CORPORATION
McDONNELL DOUGLAS RESEARCH LAB
PO BOX 516
ATTN D. P. AMES,
DEPT. H220, BLDG. 110
ST LOUIS, MO 63166

MISSION RESEARCH CORPORATION
PO BOX 279
ATTN MS. DAWN HIGGS
SPRINGFIELD, VA 22150

THE MITRE CORPORATION
TECHNICAL REPORT CENTER
ATTN DR. J. R. VAN ZANDT, H-060
BURLINGTON ROAD
BEDFORD, MA 01730

PACIFIC-SIERRA RESEARCH CORPORATION
ATTN LEONARD SCHLESSINGER
12340 SANTA MONICA BLVD
LOS ANGELES, CA 90025

PHYSICS INTERNATIONAL
ATTN EMIL KOVTUN, J. BENFORD
ATTN ALAN J. TOEPFER
2700 MERCED STREET
SAN LEANDRO, CA 94577

POWER SPECTRA INC
ATTN LARRY RAGLE
42660 CHRISTY STREET
FREMONT, CA 94538

PULSE SCIENCES INC
ATTN PHILIP D'A. CHAMPNEY
14796 WICKS BLVD
SAN LEANDRO, CA 94577

QUEST RESEARCH CORPORATION
ATTN ROBERT S. OHANESIAN
6858 OLD DOMINION DRIVE
McLEAN, VA 22101

RAND
ATTN ALEXANDER F. BREWER
1700 MAIN STREET
SANTA MONICA, CA 90406

R&D ASSOCIATES
PO BOX 9695
ATTN MR. B. MOLLER
MARINA DEL RAY, CA 90291

SAFSS
ATTN LTC MARK HODGESON
WASHINGTON, DC 20330

SANDIA NATIONAL LAB
PO BOX 969 DIV. 8341
ATTN MURRAY S. DAW
LIVERMORE, CA 94550

SANDIA NATIONAL LAB
PO BOX 5800
ATTN CHARLIE R. BLAINE
ATTN KENNETH R. PRESTWICH
ATTN MAX B. SANDOVAL
ALBUQUERQUE, NM 87185

DISTRIBUTION (cont'd)

SCIENCE APPLICATIONS, INC
ATTN LINDA WHITMEYER
1215 JEFFERSON DAVIS HIGHWAY
SUITE 310
ARLINGTON, VA 22202

SCIENCE APPLICATIONS, INC
ATTN DR. EDWARD CORNET
ATTN DR. ADAM T. DROBOT,
DIV. 157
1710 GOODRIDGE DRIVE
McLEAN, VA 22102

SCIENCE APPLICATIONS, INC
ATTN CHARLES L. YEE
5150 EL CAMINO REAL
SUITE B-31
LOS ALTOS, CA 94022

W. J. SCHAFER ASSOCIATES, INC
ATTN DOCUMENT CONTROL
1901 N. FT MYER DR.
SUITE 800
ARLINGTON, VA 22209

W. J. SCHAFER ASSOCIATES, INC
CORPORATE PLACE 128
BUILDING 2, SUITE 300
ATTN DR. JAMES P. REILLY
WAKEFIELD, MA 01880

SYRACUSE RESEARCH CORPORATION
ATTN DR. D. T. AUCKLAND
MERRILL LANE
SYRACUSE, NY 13210

SRI, INC
ATTN DR. GERALD AUGUST,
ELECTROMAGNETIC SCIENCES
LABORATORY
333 RAVENSWOOD AVENUE
MENLO PARK, CA 94025

TITAN SYSTEMS, INC
ATTN DOCUMENT CONTROL, LB
9191 TOWNE CENTRE DRIVE, SUITE 500
SAN DIEGO, CA 92122

TRW DEFENSE SYSTEMS GROUP
ATTN PRAVIN G. BHUTA,
MS 132/9085
ATTN E. V. RUTKOWSKI,
E1/1037
ONE SPACE PARK DRIVE
REDONDO BEACH, CA 90278

TRW SPACE & TECHNOLOGY GROUP
DIRECTED ENERGY LABORATORY
ATTN DR. ZAVEN G. GUIRAGOSSIAN
ONE SPACE PARK
REDONDO BEACH, CA 90278

UNIVERSITY OF MARYLAND
DEPT OF ELECTRICAL ENG.
ATTN PROF. CHI H. LEE
ATTN PROF. JEFFREY FREY
COLLEGE PARK, MD 20742

UNIVERSITY OF MICHIGAN
DEPT. OF ELECTRICAL AND
COMPUTER ENGINEERING
ATTN PROF. GEORGE HADDAD
ANN ARBOR, MI 48109

US ARMY LABORATORY COMMAND
ATTN TECHNICAL DIRECTOR, AMSLC-TD
ATTN PUBLIC AFFAIRS OFFICE, AMSLC-PA

INSTALLATION SUPPORT ACTIVITY
ATTN HDL LIBRARY, SLCIS-IM-TL (3 COPIES)
ATTN HDL LIBRARY, SLCIS-IM-TL (WOODBRIDGE)

USAISC
ATTN RECORD COPY, ASNC-ADL-TS
ATTN TECHNICAL REPORTS BRANCH,
ASNC-ADL-TR (2 COPIES)

HARRY DIAMOND LABORATORIES
ATTN D/DIVISION DIRECTORS
ATTN DIRECTOR, SLCHD-NW-E
ATTN CHIEF, SLCHD-NW-EC
ATTN CHIEF, SLCHD-NW-ED
ATTN CHIEF, SLCHD-NW-EE
ATTN DIRECTOR, SLCHD-NW-R
ATTN CHIEF, SLCHD-NW-RA
ATTN CHIEF, SLCHD-NW-RC
ATTN CHIEF, SLCHD-NW-RE
ATTN CHIEF, SLCHD-NW-RH
ATTN CHIEF, SLCHD-NW-RI
ATTN DIRECTOR, SLCHD-NW-P
ATTN CHIEF, SLCHD-RT-AA
ATTN ZABLUDOWSKI, B., SLCHD-IT-EB (GIDEP)
ATTN R. GARVER, SLCHD-NW-RE (4 COPIES)
ATTN E. BROWN, SLCHD-PO-P
ATTN J. SCZEPANSKI, SLCSM-C3I
ATTN R. CLAFFY, SLCSM-AA
ATTN A. STEWART, SLCHD-NW-P
ATTN H. DROPKIN, SLCHD-RT-RA
ATTN A. WARD, SLCHD-NW-EA (20 COPIES)

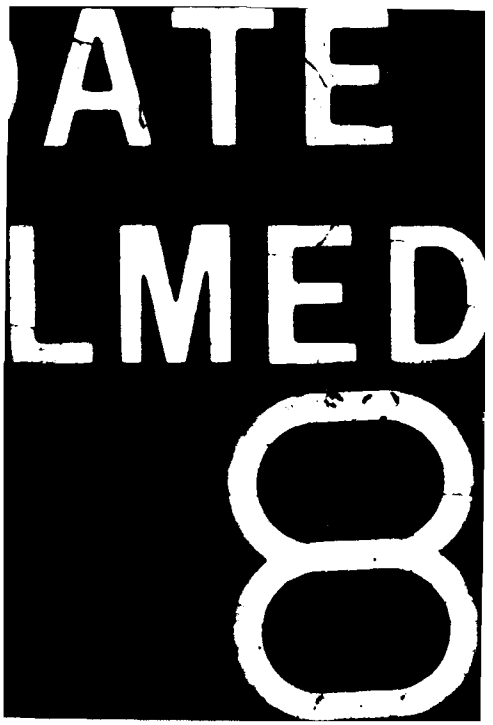
ATE
LMED
8